Ink Formulation and Selection for Biological Applications of Two-Photon Polymerization

Smita M. Panda[a†], Hossein Goodarzi Hosseinabadi[b,c,d†], Hoda Fattel[e†], Umakanta Tripathy[a], Amir K. Miri[e]*.*

[†] *Equal contributions*

* *Co-Corresponding authors*

[a] Department of Physics, Indian Institute of Technology (Indian School of Mines), Dhanbad, JH 826004, India

[b] Department of Biofabrication, Faculty of Engineering Sciences, University of Bayreuth, Ludwig Thoma Str. 36A, 95447 Bayreuth, Germany

[c] Institute of Pharmacology and Toxicology, University Medical Center Göttingen, Robert-Koch-Str. 40, 37075 Göttingen, Germany

[d] Institute for Organic and Biomolecular Chemistry, Department of Chemistry, University of Göttingen, Tammannstr. 2, 37077 Göttingen, Germany

[e] Department of Biomedical Engineering, Newark College of Engineering, New Jersey Institute of Technology, 323 Dr Martin Luther King Jr Blvd, Newark, NJ 07102, USA

ABSTRACT

Two-photon polymerization (TPP) uses nonlinear light interactions in photocrosslinkable precursors to create high-resolution (~ 100 nm) structures and high dimensional fidelity. Using a near-infrared light source in TPP results in less scattering and high penetration depth, making it attractive for creating biological models and tissue scaffolds. Due to unmatched flexibility and spatial resolution, they range from microvascular constructs to microneedles and stents. This report reviews the working principles and current inks used for TPP-printed constructs. We discuss the advantages of TPP over conventional additive manufacturing methods for tissue engineering, vascularized models, and other biomedical applications. This review will provide a short recipe for selecting inks and photoinitiators for a desired structure.

KEYWORDS: Microfabrication, two-photon polymerization, vascularized modeling, tissue engineering.

1. INTRODUCTION

Microfabrication has created scaffolds with control over microscale features such as porosity, architecture, and cellular interactions [1]. Microfabrication methods include conventional molding [2], lithography [3], and additive manufacturing [4]. The additive manufacturing method can be divided into contact-based and light-assisted methods. In contrast to contact-based methods, light-assisted methods [5], such as selective laser sintering (SLS), stereolithography (SLA), and laser-induced forward transfer, benefit from good biocompatibility, high resolution, and excellent efficiency [6]. More recently, digital light processing (DLP) [7], continuous liquid interface production [8], and two-photon polymerization (TPP) [9] have developed via selective curing of liquid polymers. This report focuses on TPP and the recent developments in the field.

The TPP offers some advantages for the fabrication of small-scale structures. The high resolution in TPP depends on the laser system, the optical design (see **Figure 1a**), as well as the ink design parameters, such as the choice of photoinitiator (PI) and the characteristics of the polymer backbone, which are below the diffraction limit and affect the photo absorption reaction [10]. The resolutions range within ~ 50-100 nm, far better than 50-100 μm in extrusion 3D printing systems and 1-50 μm in stereolithography methods. The improved resolution in TPP allows the creation of microvascular and small-structure models. In addition, it does not require cleanroom facilities or specialized equipment such as electroplating, molding, and deep reactive ion etching [11].

The translations of TPP to make tissue scaffolds and small devices have been slow and limited. There are some challenges in creating highly complex TPP-printed structures. The main challenge is the restriction over the upper size limit leading to small geometrical designs (< 2 mm thickness) [12-14]. This would impact the translation of TPP to make an organ-level model. Another drawback is the low speed compared to other 3D printing methods [12, 14, 15]. In the case

of including cells, the extended fabrication times impose the cells to be outside their optimal culture environment, which in turn causes significant stresses to the cells in the ink formulation [16]. This work reviews the fundamentals of TPP and the range of materials for biological models and medical devices. We focus on how to apply TPP for tissue scaffolds, vascularized models, and screening models. We propose some examples for future advancements and efforts to translate TPP into a tool for vascularized models. This review will help bioengineers and biomaterials scientists to select optimum inks and light properties for implementing TPP.

2. BACKGROUND

2.1. Light-Assisted Polymerization

Photopolymerization converts unsaturated molecules to solid macromolecules using photon energy. A single photon is absorbed in SLA and SLS to trigger the chemical reaction in the photosensitive medium[17]. This medium comprises a monomer or oligomer, a PI, and sometimes an optical inhibitor. The monomer is transparent to the incident light to avoid premature crosslinking. The PI absorbs the photon and triggers the polymerization process by decomposition of the PI into its constituents plus free radicals [18, 19]. The PI is excited from the ground state to the excited singlet or triplet state. There are two types of PIs in general: Type I produces reactive intermediates to initiate polymerization from the excited triplet state. Type II can abstract hydrogen from the donors and undergo a photo-induced electron transfer and fragmentation process to make reactive intermediates [20]. The reactive intermediates may be radicals or cations that initiate radical or cationic photopolymerization. These free radicals react with the monomer and form radicalized monomers, which further react with other monomer units to form a polymer chain [3].

In SLA, single photon absorption (SPA) attenuates the excitation light. The photon energy should be equal to or greater than the band gap of the PI, larger than $E_u - E_g$, where E_u and E_g

are energies of the excited and ground states, respectively (**Figure 1b**). Due to light attenuation, the photon energy will remain above this threshold only in a "voxel" around the laser focal point (**Figure 1c**). For an ink with a high concentration of PI with high optical density, the beam is highly attenuated at the surface and less effective in penetrating in a photoresist medium to photocrosslink the ink precisely at the focal length (see **Figure 1d**). For a diluted PI with low optical density, the beam intensity is maximum at the focal point and can form a gel structure at a time, as shown in **Figure 1e**. In single-photon absorption, the absorption is a linear function of light intensity which causes the resolution to be low. Because the decay of the light energy (or the decline of the threshold energy for gelation of the ink) by moving away from the focal point would be exponential. In two-photon absorption (TPA), the molecular excitation in PI can occur by absorbing two photons when the total energy of photons is greater than the band gap of the PI. The photons interact with PI molecules for a short period, and the absorption is proportional to the intensity of irradiated light to the power of two (see **Figure 1f**) [21]. Therefore, the decay would be more pronounced, allowing control of the gelation point with higher precision, leading to improved resolutions.

2.2. Two-Photon Absorption Reaction

When a PI molecule absorbs photons (either in the form of single-photon or two-photon), they lose energy, and the molecule energy moves to an upper state, where the vibrational relaxation is induced by the lowest vibrational energy level, E_l, without releasing a photon (see **Figure 1b**). Then, the state of energy returns from E_l to the ground state by a radiative pathway, leading to releasing a photon of hv' energy. A laser will provide a light intensity higher than the interatomic field strength ($E_{int} \approx 10^{11}\ Vm^{-1}$) [22] at the focal point. Considering Beer's law [5], the irradiative light intensity in z direction, $I(z)$, can be expressed in terms of the incident light intensity, I_0, as shown in **Equation 1** [3].

$$\begin{cases} \text{for SPA:} & I(z) = I_0 e^{-\ln(10)\varepsilon c z} \rightarrow \frac{dI(z)}{dz} = -I(z)\varepsilon c \ln(10) \rightarrow P \propto I \\ \text{for TPA:} & I(z) = \frac{I_0}{1+\beta z I_0} \rightarrow \frac{dI(z)}{dz} = -I(z)^2 \times \beta \rightarrow P \propto I^2 \end{cases} \quad (1)$$

here, ε is absorptivity, c is the concentration of photoinitiator, z is the depth into the ink, β reflects the two-photon absorption coefficient, and P is the probability of absorption of the incident light [19]. In the case of two-photon absorption reaction, Maria Göppert-Mayer showed that if two photons of around equal low energy interact with a molecule nearly simultaneously, *i.e.,* at $\sim 10^{-16}$ s, they can theoretically produce an excitation equal to that of interaction between the molecule and a single photon with twice the energy of those low energy photons [23, 24]. Then, the probability of occurrence of these simultaneous two photo absorptions leading to the excitations, P, would be a 'nonlinear' phenomenon because the rate at which they occur at that time scale depends nonlinearly on the rate or intensity of the incident photons (**Equation 1**). Intensity is the number of photons that pass through area per second, while power is energy per second. Since intensity depends on the area, it is greater at the focal point than a distance away, while the power is almost the same everywhere along the laser beam. The TPA absorption energy, *i.e.,* the energy of simultaneous absorption of two photons by a PI molecule, quadratically depends upon the local incident light intensity, leading to a higher resolution. By linear moving from the focal point, the exposed area to the incident laser beam expands, leading to linear decrease of the incident laser intensity (I_i). However, the TPP excitation intensity would be proportional to the square of the incident light intensity (I_i^2). In TPP only a limited volume, 'voxel,' of the ink around the focal point will be exposed to enough irradiation (*i.e.,* threshold dose) to initiate the photocrosslinking. As a result, TPA reaction can provide far better resolution for 3D printing than SPA reaction. In the contrary, in the SPA with a gaussian nature (which is the case in DLP and other light-assisted methods based on the single photon), the decay of the excitation intensity by moving away from the center of the focal point would take place linearly with the decline of the intensity of the focused laser (**Equation 1**). The laser

intensity decreases proportionally to increase the cross-section area of the beam with a Gaussian profile. This returns a larger voxel and weaker resolution in SPA (**Figure 1b**).

Focusing the laser beam alone is insufficient to sufficiently increase the probability that two photons simultaneously interact with a molecule. A pulsed laser can be used to increase these probabilities further. A pulsed laser such as the mode-locked titanium sapphire (Ti:S) laser can produce above 80 million pulses per second, each with a pulse duration of around 100 fs. Compared to continuous wave lasers, a typical pulsed laser can theoretically increase the probability of two-photon emissions from 20'000 to 2 billion photons per second [23].

2.3. Two-photon Polymerization (TPP) Process

When laser light is exposed to the ink material, due to the nonlinear property of the optical process it tightly focuses onto a spot forming a small building block of 3D structure, called volume pixel or 'voxel' [25]. The excitation in TPA is confined to the voxel around the focal point as analytically defined in **Figure 1c**. The shape of a voxel is like an ellipsoid. The shape and size of the voxel and laser intensity distribution depend upon the parameters such as objective numerical aperture (NA), laser mode, and refractive index difference between the immersion system and photosensitive molecules [25, 26]. The PI generates radicals in a highly localized region around the center of the beam [27, 28]. The TPP requires femtosecond lasers, and a high laser intensity can produce features below the diffraction limit by regulating the quantity and energy of the laser impulses [29, 30]. The polymerization process is initiated by exposure to high-intensity laser energy, and it occurs inside a reaction threshold area of a Gaussian-like form. The transition from one-photon to two-, and then three-photon absorption can decrease the threshold for the polymerization area or voxel size [31].

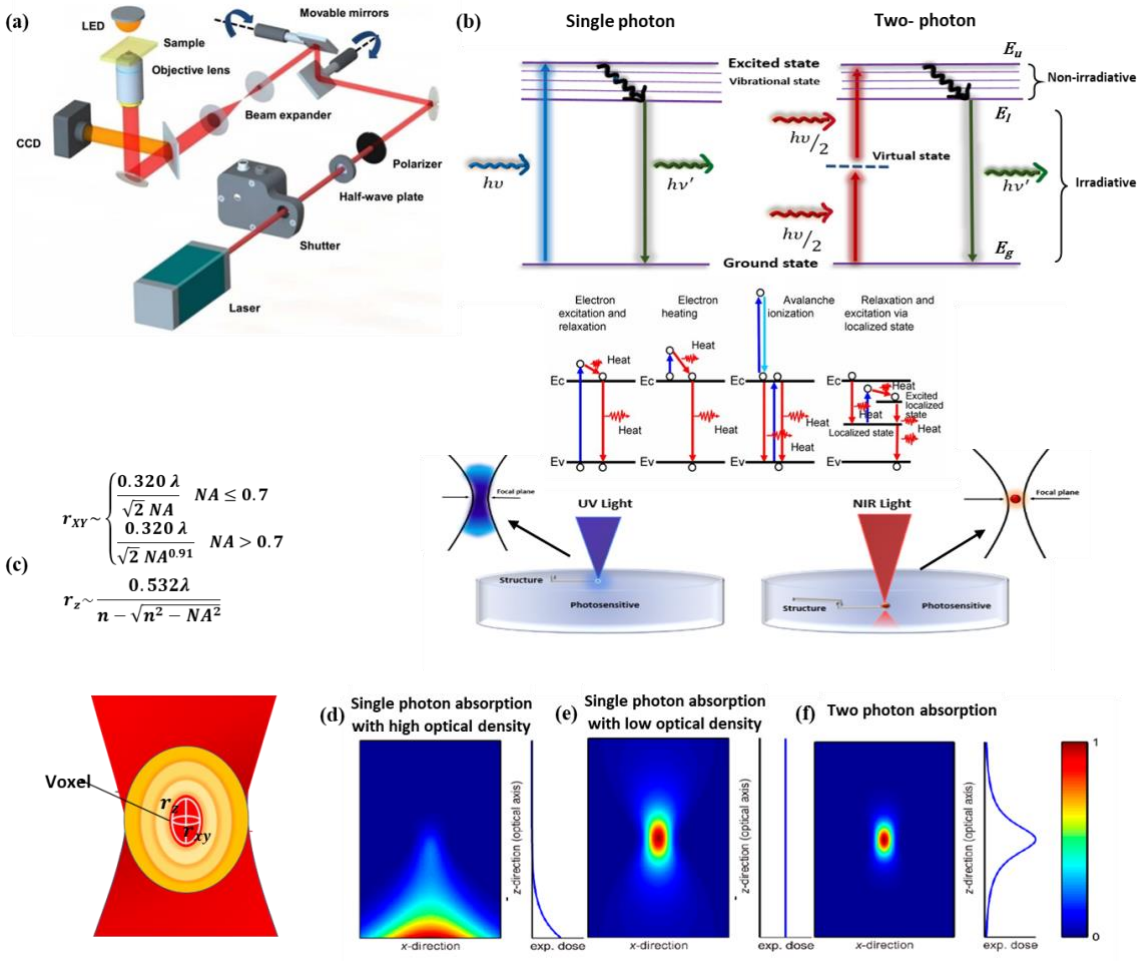

$$r_{xy} \sim \begin{cases} \frac{0.320\,\lambda}{\sqrt{2}\,NA} & NA \leq 0.7 \\ \frac{0.320\,\lambda}{\sqrt{2}\,NA^{0.91}} & NA > 0.7 \end{cases}$$

$$r_z \sim \frac{0.532\lambda}{n - \sqrt{n^2 - NA^2}}$$

Figure 1- a) Schematic of the TPP process (Reproduced with permission from ref. [32] Copyright [2017] [John Wiley and Sons]), **b)** comparing the excitation volume of single-photon absorption, and TPA due to possible mechanisms such as thermal heating or avalanche ionization (adopted from Wu et. al [33]), **c)** diagram of a voxel in TPP, **d, e, f)** Illustration of laser intensity profile taken from Ref. [34] with permission.

The highest absorption is at high-magnification focus, in which a Gaussian laser beam profile with an intensity distribution $I(r,z)$ at distances from the center (z in the direction of propagation and r along the cross-section) can be defined as [35]:

$$I(r,z) = I_0 \left(\frac{\omega_0^2}{\omega(z)^2}\right) e^{-\frac{2r^2}{\omega(z)^2}} \quad (2)$$

where I_0, ω_0, and $\omega(z)$ are the intensity at the center of the Gaussian beam ($r = 0,\ z = 0$), the waist of the beam, and the radius of the beam in the plane with a distance of z, respectively (**Figure 1c**). The photon-polymerization starts when the density of radicals $P_{(r,z)}$ exceed the threshold P_{th} ($P_{(r,z)} \geq P_{th}$). At the focal plane ($z = 0$), the intensity reaches the threshold:

$$I(r,z) = I(r,0) = I_0 e^{-\frac{2r^2}{\omega_0^2}} \quad (3)$$

A high NA objective lens can be used for closely focusing the laser onto the ink, which enables achieving a high photon density near the focal point to fabricate sub-micron structures. The voxel size is proportional to $\frac{1}{(NA)^4}$; thus, a high NA value leads to superior resolution in TPP. The resolution also depends on wavelength. Its axial (r_z) and lateral resolution (r_{XY}) are fundamentally governed by Abbe's Law [21]. **Figure 1 (c)** shows the dependence of voxel parameters on NA and wavelength [23].

The directionality of light and scattering level can control the resolution of the TPP structure, which is primarily influenced by the size of the light-cured voxel. The voxel size can be adjusted by modifying the laser's parameters (i.e., pulse width, light wavelength, power, repetition rate, and beam size) and the ink's properties (i.e., viscosity and yield stress). If E_i is the irradiation of light ($\frac{mJ}{cm^2}$), and E_c is the threshold value of the energy of the gelation point for the liquid ink ($\frac{mJ}{cm^2}$), the ink gets solidified when E_i approaches E_c, and the layer is cured. The height of the light-cured voxel is defined by [36]:

$$C_d = D_p \ln \frac{E_i}{E_c}, \quad (4)$$

Here, C_d is the depth of curing (μm) and D_p is the depth of light penetration (μm). The ink optical properties decide the selection of the laser intensity.

3. TPP Inks

The physical and biomechanical properties of the TPP-printed constructs can be controlled by proper selection of the ink composition including both the ink monomer/oligomer and PI component. A list of the used photopolymer inks and their relevant PIs, biodegradability, and biocompatibility are shown in **Table 1** to assist proper selection of the ink composition for tailored applications.

In TPP, when the ink composition is exposed to the focused laser light, the light-absorbing molecules absorb the photons from the incident laser beam. Due to this absorption, the molecules undergo a photochemical reaction, leading to the generation of additional photons. These generated photons contribute to the polymerization process, facilitating the formation of the printed constructs. The emitted photons play a role in influencing the physical properties of the TPP printed constructs, as well as their biocompatibility. The interaction between the absorbed and emitted photons and the ink composition can impact factors such as polymerization efficiency, resolution, mechanical strength, and biocompatibility of the final printed structures. The irradiation energy for photopolymerization should be kept below a threshold for biological samples to satisfy the cell compatibility.

Table 1. Some photosensitive materials used in TPP.

PI	WS	Photopolymer	BD	BC	Ref
Irgacure 127	N	OrmoComp hybrid polymer	N	Y	[37]
		Ormocer organically modified ceramic	N	Y	[38, 39]

Irgacure 369	N	Ormosil organically modified silica	N	Y	[40]
		Methacrylated urethane	N	Y	[41]
		PEGDA (M_n:700)	N	Y	[41]
		Methacrylated branched polylactide	Y	Y	[42, 43]
		PEGDA (M_n:742)	N	Y	[43]
Irgacure 819	N	PETA, BisGMA (80:20)	Y	Y	[44]
Irgacure 2959	Y	HAMA	Y	Y	[45]
		Allyl-chitosan (6 wt%),	Y	Y	[46]
Irgacure 2959	Y	GelMAAm	Y	Y	[47]
Rose Bengal	Y	Fibronectin	Y	Y	[48]
		Bovine serum albumin	Y	Y	[48, 49]
		Collagen	Y	Y	[49, 50]
		Fibrinogen	Y	Y	[48, 51]
Riboflavin, TEA	Y	PEGDA (M_n:742)	N	Y	[27]
DEABP	N	PCLcoTMC -b-PEG-b- PCLcoTMC	Y	Y	[52]
-	-	Zr-Si polymer ceramic	N	Y	[46, 53-56]
FAD	-	BSA	Y	Y	[57, 58]
Methylene blue	Y	Lyophilized BSA	Y	Y	[59]
Eosin	Y	Lyophilized BSA	Y	Y	[59]
VA-086	Y	GelMA	Y	Y	[60]
LAP	N	SZ2080 ™	N	Y	[61]

WS: water soluble, BD: biodegradable, BC: biocompatible/non-toxic, PEGDA: polyethylene glycol diacrylate, PETA: pentaerythritol-triacrylate, BisGMA: bisphenol A glycidyl methacrylate, HAMA: hyaluronic acid methacrylate, GelMAAm: gelatin methacrylamide, PCLcoTMC: poly(ε-caprolactone-co-trimethylenecarbonate), PEG: polyethylene glycol, BSA: bovine serum albumin, GelMA: gelatin methacryloyl, TEA: triethanolamine, DEABP: 4,4'-bis(diethylamino)-benzophenone, FAD: flavin adenine dinucleotide.

The laser source is typically a Ti:S femtosecond laser with nearly 800 nm wavelength. Other laser types, e.g., Yb-based femtosecond lasers or picosecond lasers, are also available for TPP. Because of lack of TPP-specific PIs, PIs for single photon polymerization, such as Irgacure 369 and Irgacure 2959 (515 nm) were initially used in TPP process [62]. Such initiator molecules usually have a low TPA cross-section (< 40 Goeppert-Mayer, GM) which makes them of limited initiation efficiency. Therefore, relatively long exposure time and high laser energy were required to achieve polymerization, especially for the typical wavelength of 800 nm [63]. A list of different types of PIs and the wavelength for their implementation in a variety of light-assisted 3D printing techniques are summarized in **Tables 2**. Only few PIs are exclusively developed to be utilized efficiently in TPP. A deep understanding of the relationship between the PI molecular structure and the TPA reaction is required to make strategies for developing proper PIs toward TPP. Eventually, some recent studies show non-photosensitized inks also can be structured with TPP even without the addition of PIs, as shown in Table 2, resulting in enhanced biocompatibility and decreased autofluorescence (see Butkus et al. [64]).

Table 2. PIs used in light-assisted polymerization [63].

PI	Type of initiator	Maximum Absorbance	Wavelength
Irgacure	Type I	276 nm	365 nm
TPO	Type I	267, 298, and 380 nm	-

LAP	Type I	375 nm	320-390 nm, 405 nm
BAPO-OLi	Type I	375 nm	320-420 nm
VA-086	Type I	365 nm	365-385 nm
Eosin-Y	Type II	528 nm	400-800 nm
Riboflavin	Type II	223, 267, 373, and 444 nm	300-500 nm
P2CK	Type II/ TPP	800 nm	-
WSPI	Type II/ TPP	800 nm	-

TPO: diphenyl (2,4,6-trimethylbenzoyl) phosphine oxide, BAPO: bisacylphosphine oxide, LAP: Lithium phenyl-2,4,6-trimethylbenzoylphosphinate.

The molecular structures of some selected PIs used in TPP are shown in **Figure 2**. The key aspects of proper PIs are: I) the chromophoric groups with large TPA regions, II) the chemical functionality with proper initiation efficiency (i.e., high radical yielding), and III) the mechanism of chemical function activation by chromophores excitation [65-67]. The PI with a large TPA and high initiation efficiency maybe insufficient for biological hydrogel-based models. As implied in **Table 1**, biocompatibility and acceptable water solubility provide a minimized cytotoxicity which are among other factors needed to be taken care of during ink selection.

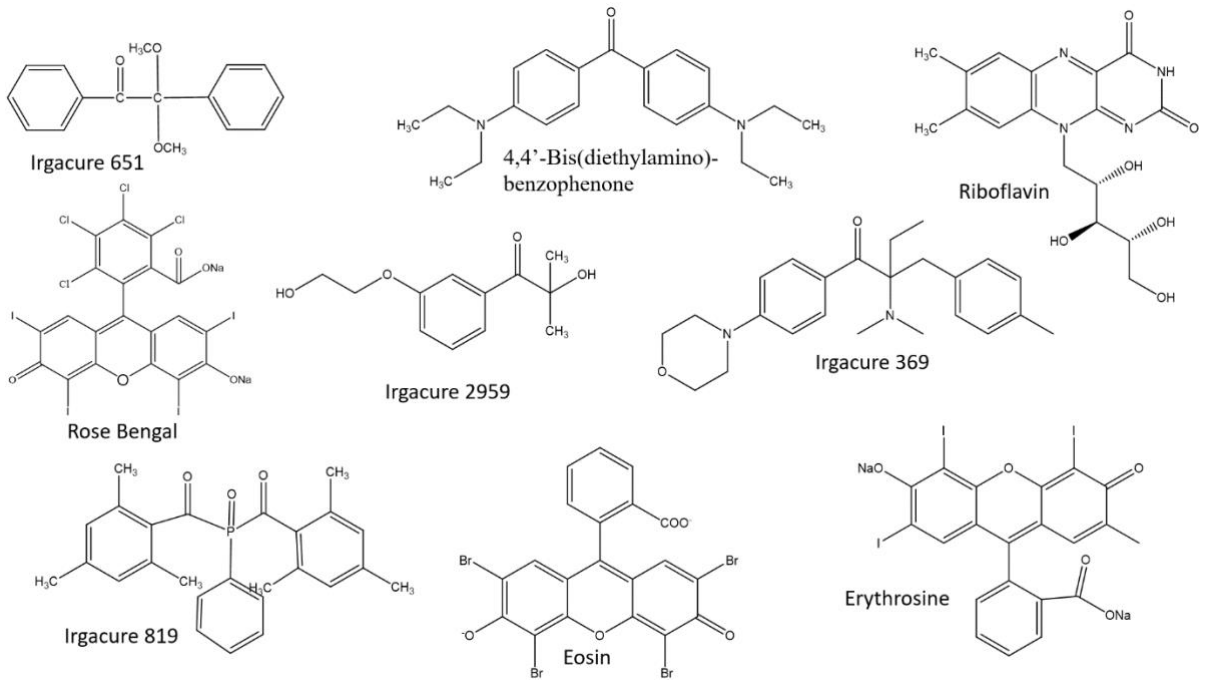

Figure 2. Molecular structures of selected PIs widely used in TPP.

Most of available PIs cannot be used in TPP 3D printing of cell-laden and biomedical samples. Type-I PIs are mostly not biocompatible [68], and researchers have given efforts towards the development of type-II PIs. Among type-II photoinitiators, WSPI (1,4-bis(4-(N,N-bis(6-(N,N,N-trimethyl-ammonium)-hexyl)-amino)-styryl)-2,5-dimethoxybenzene tetraiodide), π-Expanded Ketocoumarins [69], P2CK (sodium 3,30-(((1E,1E0)-(2-oxocyclopentane-1,3-diylidene)bis(methanylylidene))bis(4,1-phenylene))bis(methylazanediyl) dipropanoate) and T1-T3 (a series of water-soluble benzylidene cyclone dyes) [70] are considerable. Taking into account its less complicated synthesis method and its high initiation efficiency (TPA cross-section around 140 GM at 800 nm), P2CK has been the most commonly applied PI in TPP in recent years [20]. However, it is not suitable to be processed together with cells in cell-(bio)printing. It can penetrate the cell membrane and, in the presence of laser irradiation it produces singlet oxygen that is toxic to cells [71, 72].

Most of the commercial PIs require UV light sources, and their absorption cross-section in the near-infrared region, which is usable for TPP, is very small. In other words, monomers often do not absorb the laser light in the TPP range to a significant extent. Adding photosensitizers can be a strategy to increase the absorption efficiency in the near-infrared region. A photosensitizer can absorb light and transfer that energy to another molecule, i.e. monomer, to start a photoreaction. Separate from photosensitizers, the monomers used in TPP are mostly comprised of acrylic-based materials. There are some low-cost and readily available inks, e.g., inorganic-organic hybrid materials (Ormocers) [28], acrylic-based prepolymers [73], urethane acrylate monomers [74], gelatin hydrogels [75], and zirconium sol-gels [76]. One possible mechanism of light interaction is also through dielectric breakdown or avalanche ionization within the monomer without PI [68]. Even though this method is enticing from a biocompatibility point of

view, TPP would have a very narrow working range. Another is through the radical formation and initiation efficiency, which affect the laser requirements [68]. The PI should efficiently work in a wide range of TPP printing speeds and laser powers to make fabrication more flexible and effective. A high degree of conversion leads to decreased residual monomer and fast polymerization kinetics, thus causing quicker polymerization.

4. TPP-Printed Models

4.1. Scaffold Design

TPP holds significant potential in the tissue engineering field, where scaffolds have been manufactured with desired pore sizes, interconnectivity, and gradients using biocompatible materials [77] (**Table 3** and **Figure 3**). The ink monomers can be extracted from naturally derived components or can be fully synthetic. The common examples are poly-ethylene-glycol diacrylate (PEGDA) and GelMA [78, 79]. Inks should show some features for scaffolding. Biodegradation, the natural process of water solubilizing a material in the body that causes the material to break down, is a key feature for the design of many scaffolds. Biodegradation rates from several hours to days would make them suitable for tissue regeneration in various organs [80, 81]. The other property is the ink's mechanical strength, which might be correlated with biodegradation rates [80]. These properties should be assessed using different combinations to mimic the target tissue. They also need to possess biocompatibility properties, meaning that the biomaterials should have low to negligible toxicity to the cells and other tissues [81]. Varying all the properties enables scaffold design with the desired features in the tissue engineering field. There have been several bold studies in using TPP for fabrication of scaffolds, as summarized in **Table 3**.

Table 3. Selected TPP made scaffolds using natural and synthetic biopolymers.

Material	PI	Application	Cell Type	Laser Properties	Advantages	Ref
GelMOD	Irgacure 2959	Scaffold	Porcine Mesenchymal Cell	Ti:S (200 fs, 3.5 mW, 1 MHz, 515 nm).	Support porcine MSC adhesion and differentiation into osteogenic lineage 1.5 µm resolution	62
PEGDA	Irgacure 819	Scaffold	Neuro2A cell	Femtosecond (100 fs, 50 mW, 940 nm)	Neuronal architecture Growth of multiple neurotic extensions, 20 µm resolution	82
PETA	4MetBAC	Scaffold	Human dermal fibroblasts	Femtosecond (0.9 mW, 780 nm)	Optoelectronic and biological applications, polymerization threshold is 0.9 mW 72 nm resolution	83
Silk Fibroin	Ruthenium	Scaffold	Human dermal Fibroblast	IR Ti:S (140 fs, 800-2400 mW, 80 MHz, 800 nm)	Gradient mechanical and chemical properties, high viability, resolution, and resistance to enzymatic degradation	84

AKRE and ORMOSIL	N/A	Scaffold	Adult stem cell	Ti:S (80 fs, 500 mW, 80 MHz, 800 nm)	Biocompatibility	[85]
GelMA	P2CK	Scaffold	Human BJ foreskin fibroblasts	Erbium-doped (100-200 fs, 150 mW, 780 nm)	Lateral and axial resolution of 6 µm Low cytotoxicity	[75]
Chitosan	Irgacure 2959	Scaffold	HPMEC	Ytterbium (250 fs, 300 mW, 21 MHz, 520 nm)	No cytotoxicity Tunability	[86]
Methacrylated branched polylactide	Irgacure 369	Scaffold	human neuronal and rat Schwann	Ti:S (120 fs, 80 MHz, 780 nm)	Neural tissue engineering, 20 µm resolution	[42]
PETA, BisGMA (80:20)	Irgacure 819	Scaffold	NBDS cell	Ti:S (150 fs, 15-20 mW, 80 MHz, 800 nm)	35 µm square pore size scaffold	[87]
HAGM, PEGDA (HA-PEG)	Irgacure 2959	Scaffold	Human fibroblasts & osteoblast	Ytterbium (250 fs, 300 mW, 21 MHz, 520 nm)	Mechanically stable scaffold, biocompatible with osteoblasts	[45]

Allyl-chitosan (6 wt%), HAMA (2 wt%)	Irgacure 2959	Scaffold	Hippocampal cell	TEMA100 (525 nm)	Facilitated the formation of nerve cells, low cytotoxicity	[46]
Gel-MAAm	Irgacure 2959	Polymer–protein hybrid microstructures	Chondrocyte	Ti:S (100 fs, 3000 mW, 80 MHz, 690-1040 nm), Frequency-doubled μ-chip Nd:YAG (25 mW, 7 kHz, 532 nm)	Strong cell growth characteristics, 1.2 μm resolution	[47]
Fibronectin	Rose Bengal	Polymer–protein hybrid microstructures	Chondrocyte	Ti:S (100 fs, 3000 mW, 80 MHz, 690-1040 nm) Nd:YAG μ-chip (25 mW, 7 kHz, 532 nm)	No disruptions or significant deformation during shrinkage, 30 μm resolution	[47]
BSA	Rose Bengal	Protein	N/A	NIR Ti:S (100 fs, 120	Entrapment of bioactive compounds that	[48, 49]

		Microstructure		mW, 76 MHz, 700-1000 nm)	diffuse from a polymer matrix	
Collagen	Rose Bengal derivative	Protein Microstructures	N/A	Ti:S (100 fs, 50 mW, 76 MHz, 780-850 nm)	Kinetics reduced, stable structures	[49, 50]
Fibrinogen	Rose Bengal	Protein Microstructure	N/A	NIR Ti:S (200 fs, 5.2-15.7 Mw, 700-980 nm)	1-3.8 µm resolution	[48, 51]
PCLcoTMC-b-PEG-b-PCLcoTMC	DEABP	Scaffold	Balb/c 3T3 NIH cell	Ti:S (20 fs, 450 mW, 75 MHz, 800 nm)	4 µm resolution, No cytotoxicity: no detrimental effect on cell proliferation	[52]
BSA	FAD	Protein Microstructures	Neuroblastoma-glioma & brain cortical cell	Ti:S (30-60 mW, 740-790 nm)	Cortical neurons, Low cytotoxicity, < 5 µm resolution	[57, 58]
Lyophilized BSA	Methylene blue	Protein Microstructures	PA cell	Ti:S (5–25 mW, 740 nm)	Translational and rotational degrees of freedom, flexibility in shape < 1 µm resolution	[59]
Lyophilized BSA	Eosin	Protein Microstructures	PA cell	Ti:S (5–25 mW, 740 nm)	Translational and rotatio2Pl degrees of freedom, flexibility in shape, < 1 µm	[59]

	resolution

N/A: not available, Ti:S: titanium sapphire, NIR: near infrared, HAGM: glycidyl methacrylated hyaluronic acid, HPMEC: human pulmonary microvascular endothelial cells, MSC- Mesenchymal stem cell, 4METBAC- α,α-bis(arylidene)cyclopentanone, NBDS – Nonbulbar dermal sheath, HGMA-Hyaluronic acid-glycidyl methacrylate, PA- Pseudomonas aeruginosa cell line.

Ovsianikov et al. developed a scaffold with a 10 by 10 pore array (250 μm × 250 μm, spaced at 300 μm) using methacrylamide-modified gelatin (GelMOD) with PI Irgacure 2959 as shown in **Table 3** [62]. The osteogenic simulation was then tested on the scaffold with porcine mesenchymal stem cells [62]. Accardo et al. developed a 3D scaffold made of PEGDA, PI Irga 819, and neuroblastoma cell line (neuro2A cells) using two-photon lithography direct laser writing to form neuritic extensions or interconnections [62]. The scaffold had a 280 (x) × 280 (y) × 280 (z) μm^3 overall size with a woodpile configuration made of cylindrical sub-units (20 μm diameter, 20 μm vertical spacing, 60 μm horizontal spacing) [60]. The resulting scaffold provided a favorable environment to the cells in neuroscientific applications involving neural tissue engineering. Zhigansha et al. developed a new component methacrylate containing PI 4MetBAC, which was deemed safe and biocompatible when tested with monomer Pentaerythritol tetraacrylate (PETA), human dermal fibroblasts, and HEK29 cells through TPP at a 780 nm wavelength to develop a 30 μm period (wall width is approx. 2 μm) scaffold as shown in **Table 3** [83]. In another study, Valente et al. used TPP to control the crosslinking degree of silk fibroin with ruthenium by regulating the laser intensity between 800 and 2400 mW, resulting in a scaffold of 100 μm × 100 μm x 10 μm with different degradation rates from 0.5 to 2 hours and stiffness from 9.6 to 47.2 kPa [84]. The authors also showed a decreasing average pore area from 1.13 to 0.25 μm^2 while increasing the laser power fom 800 to 2400 mW. In addition, the hydrogel showed high cell viability (over 95% during 21 days) and proliferation rate when combined with human dermal fibroblasts. TPP is an effective bioprinting method to construct scaffolds of different sizes at the microscale with varying stiffness, pore size, and degradation rates, holding potential for biological and clinical applications.

4.2. Vascularized Models

Capillary modeling in tissue engineering involves blood vessels with sizes ranging from 5 to 50 μm. Microfluidic devices emerged to gain insight into the cellular dynamics in microvascular remodeling in vitro while using less volume of samples and reagents. Alsharhan et al. utilized TPP to fabricate 3D static interwoven micro-vessel-inspired structures with inner diameters as small as 8 μm using cyclic olefin polymer (COP) [88]. Moreover, Van der Valden et al. focused on achieving an organ-on-chip through TPP with defined pores of 250 nm, a width of 100 μm, a height of 10 μm, and a length of 350 μm [89]. They concluded that the maximum voxel diameter must be considered for fabricating high-resolution pores. Microfluidic devices are popular methods to mimic microvessels in the neurological field and the blood-brain barrier model. Marino et al. fabricated a 1:1 scale, biomimetic, and biohybrid blood-brain barrier model with microcapillaries of an average diameter of 10 μm, pore size of 1 μm, and length of 63.6 μm [90]. TPP allowed the model to fine-tune different microfluidic parameters such as pore and micro-capillary diameter, pore density, and porous segment length. This model opens doors to drug treatments and therapeutic studies of the brain pathologies such as brain cancer. Trincini et al. constructed a microfluidic device consisting of an array of ten microtubes of a length of 1.1 mm, having capillaries of 50 μm in diameter. The capillaries at the ends (150 μm in length) are non-porous, while the central one (800 μm in length) is porous (5 μm in diameter). The authors proved that their 1:1 scale 3D-printed realistic biohybrid model of the brain tumor microenvironment can hinder dextran diffusion and enable chemotherapy-loaded nanocarriers to cross the barrier, meaning that the model can be used for high throughput drug screening [91]. Hence, TPP enables the manufacturing of *in vitro* microcapillaries to scale, providing a realistic model for therapeutic and diagnostic applications in nanomaterials and biomedicine.

4.3. Drug Testing Applications

Previous studies created 400 µm microcarriers for high-throughput cell analysis much larger than the average cell size (10 µm) [92]. Using a scanning two-photon continuous flow lithography technique, Chizari et al. [93] fabricated a 50 µm cell carrier microparticle using a femtosecond pulsed laser with 20 mW with a throughput of 10 microparticles per second (**Figure 3a**).

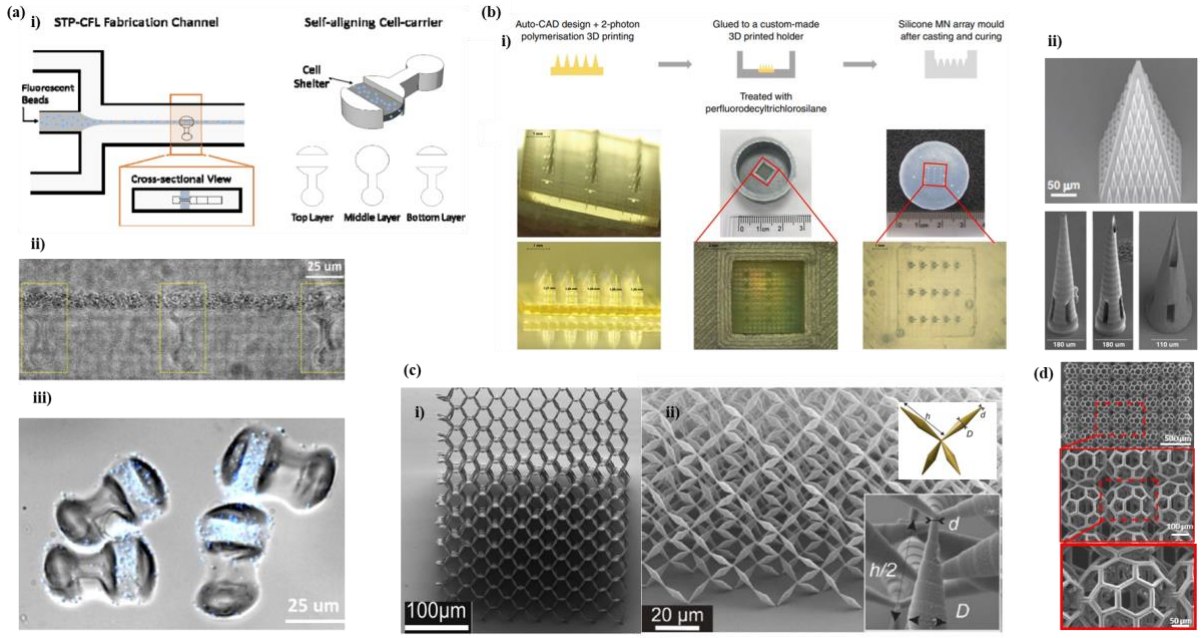

Figure 3. Some applications of TPP in form of: a) multi-functional microparticles as self-aligning cell-carriers taken from Ref. [93], b) microneedle arrays for transdermal delivery with molding (i) (Reproduced with permission from ref. [94] Copyright [2017] [John Wiley and Sons]) and without molding (ii) [95], c) pentamode mechanical metamaterials as biomedical devices (Reproduced with permission from ref. [96] Copyright [2012][AIP Publishing]), d) a biodegradable array of buckyball-shaped scaffold for tissue engineering taken from Ref. [14].

The integration and precise placement of materials at small scales continue as a challenge in manufacturing micro- and nanoparticles. Kesteren et al. combined TPP with capillarity-assisted particle assembly to overcome this challenge and obtain multi-material microstructures. In this

case, the TPP plays an essential role in the realization of traps with 3D profiles needed for the co-assembly of microparticles and the printing of links that attach the particles from single units to millimeter-scale lattices[97].

Another potential use of TPP in biomedical application is micro stents. The ineffective available fabrication techniques impede making small scale 3D microstates with a high shape-morphing freedom. Jin et al constructed microstents with line widths of ~250 nm made of acrylic acid (AAc) and N-isopropylacrylamide (NIPAAm) with uniaxial contraction through DLW, which employs TPP. They show that the exposure dosage of femtosecond laser pulses modulates the material crosslinking densities, stiffnesses, and swelling/shrinking degrees [98]. The printed sample had a stiffness of 25 N/m with a laser power of 12mW (24% of the maximum laser power). Its stiffness continuously elevated till 400 N/m at 35mW, 70% of the maximum laser power. Another study created 3D cylindrical structures with line widths of ~250 nm to analyze cancer cells' behavior and migration in the presence of porous scaffolds with tunable stiffness. The cylindrical microstructure designs had three main features: size enabling cancer cell invasion, the porosity of the lateral surface allowing the transfer of cell culture medium, and ease of fabrication. Structural stability and porosity on the lateral surface of the cylinder were attained through the repetitive basic zigzag unit design. It is known that cell behavior is strongly influenced by the biophysical cues of the environmental, mechanical properties. Furthermore, cell adhesion requires substrate stiffness to drive the cell's motility and invasive behavior. The fabricated microstructures resulted in a stiffness of 2.7 GPa, 3.7 GPa, and 4.7 GPa with a constant laser power of 45%, 65%, and 85% of the maximum power (20mW). They tested human colorectal adenocarcinoma (LS-174T) tumor cell invasion on the printed cylindrical stent-like structures and found that the stiffer microstates are less invaded than, the softer ones [99]. There is a direct relation of laser power and stiffness in TPP, which proves to be a useful application in micro stents.

TPP has also been used to produce microneedles or microneedle arrays with a resolution down to a 100 nm [100] (**Figure 3b**). Microneedles are used in the drug delivery and vaccination field to deliver nanoparticles to the epidermis or the dermis layer of the body using a minimally invasive technique. Factors such as shape or conformation of needle structure and mechanical strength can affect the efficacy of the microneedle [101]. Unlike reactive ion etching, lithography-electroforming-replication, and other conventional microelectronics-based technologies, TPP fabricates microneedles with a wider range of geometries such as in-plane, out-of-plane, mosquito fascicle-shaped, and rocket-shaped microneedles [102]. Cordeiro et al. demonstrated that sharp conical and pyramidal needles exhibited the highest insertion depth value (64-90% of needle height) using TPP, which resulted in higher drug delivery rates [94]. One issue with the current conventional materials and methods is the poor fracture behavior of the fabricated microneedle. Gittard et al. used TPP and subsequent polydimethylsiloxane (PDMS) micromolding to create acrylate-based polymer hollow microneedles for transdermal delivery [103]. The microneedle array could withstand an axial load of 10 N (0.4 N per needle), which is seven times greater than the required force for microneedle insertion into the skin (1.29 N). This demonstrates that TPP provides suitable compressive strength for microneedles for transdermal drug delivery applications.

Figure 4 summarizes several developments made in the past decade to improve the fabrication speed and size of the features built by TPP. In the past decade, industrial applications of TPP have been limited mostly due to suffering from either small fabrication speeds or size of the features could be produced by the technique. In recent years, the fabrication speed is significantly increased which is promising for possible commercial application of the TPP in future. Weisgrab et al. [14] have reached up to 1000 mm/s fabrication speed (see **Figure 4**) which is close to the high fabrication speeds of techniques such as SLA and DLP 3D printing [104-107]. They have shown production of relatively large features (~300 mm^3) with a highly complex

metamaterial architecture at the high fabrication rate (see **Figure 3d**). At this speed levels, fabrication of cellular structures for building micro-tissue models is expected which can become a mainstream in the next decade with plenty of potentially clinical or drug-screening applications [105].

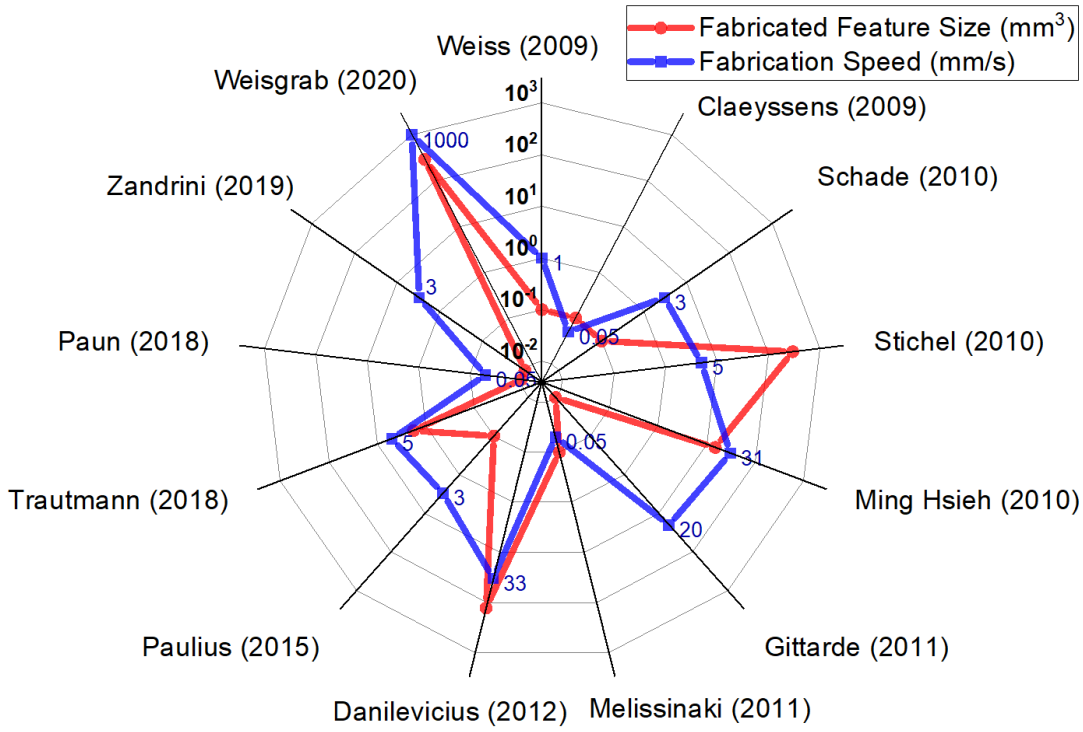

Figure 4. Developments in the speed and volume of the fabricated features by TPP [13-15, 52, 108-114].

5. Summary

This review summarizes the concept of TPP, a fabrication method for 3D micro/nanostructures with high feature resolutions beyond the diffraction limit. In recent years, TPP has shown great flexibility compared to conventional microfabrication techniques in optics, microelectronics, metamaterials, tissue engineering, 3D scaffold design, biomimetics,

drug delivery, etc. Even though TPP has shown promising results, more work must be done to overcome the current challenges of slow fabrication speed, material toxicity, and expensive equipment. For example, commonly used polymers may be non-toxic; however, unreacted monomers, oligomers, and PIs may be toxic. This biocompatibility issue can be averted using biological polymers with photochemical and water solubility properties. The fabricated structure can also be improved in size by extending it beyond micro to centimeters with high submicron resolution. We expect that there will be significant improvements in the near future with the help of computational modeling, technological progress, and continuous research on the response of cells and their microenvironment to new TPP materials.

CORRESPONDING AUTHORS

Dr. Amir K. Miri, PhD

e-mail: am3296@njit.edu; Phone: 973-596-6366

Postal Address: 323 Dr Martin Luther King Jr Blvd,

Fenster Hall 624 (BME), Newark, NJ 07102-1982, USA

Dr. Umakanta Tripathy, PhD

email: utripathy@iitism.ac.in, Phone: 91-9471192489.

Postal Address: 826004, Jharkhand, India

CRediT authorship contribution statement

Smita M. Panda: Conceptualization, Investigation, Visualization, Resources, Writing – original draft, review & editing, Formal analysis.

Hossein Goodarzi Hosseinabadi: Investigation, Formal analysis, Writing – review & editing.

Hoda Fattel: Investigation, Visualization, Resources, Writing – original draft.

Umakanta Tripathy: Conceptualization, Supervision, Project administration, Funding acquisition, Writing – review & editing.

Amir K. Miri: Conceptualization, Supervision, Project administration, Funding acquisition, Writing – review & editing.

Declaration of Competing Interest

The authors declare that they have no known competing financial interests or personal relationships that could have appeared to influence the work reported in this paper.

Acknowledgements

S.M.P. acknowledges Indian Institute of Technology (Indian School of Mines), Dhanbad, India for institute fellowship and infrastructure facilities. H.G.H. acknowledges the receipt of fellowship award by the Alexander von Humboldt Foundation during this research. A.K.M. acknowledges the receipt of a start-up fund from NJIT and the grant no. R01-DC018577 from NIH.

REFERENCES

1. Gauvin, R.; Chen, Y.-C.; Lee, J. W.; Soman, P.; Zorlutuna, P.; Nichol, J. W.; Bae, H.; Chen, S.; Khademhosseini, A., Microfabrication of complex porous tissue engineering scaffolds using 3D projection stereolithography. *Biomaterials* **2012,** *33* (15), 3824-3834.
2. Maruo, S.; Fourkas, J. T., Recent progress in multiphoton microfabrication. **2008,** *2* (1-2), 100-111.
3. Sun, H.-B.; Kawata, S., Two-Photon Photopolymerization and 3D Lithographic Microfabrication. In *NMR • 3D Analysis • Photopolymerization*, Fatkullin, N.; Ikehara, T.; Jinnai, H.; Kawata, S.; Kimmich, R.; Nishi, T.; Nishikawa, Y.; Sun, H. B., Eds. Springer Berlin Heidelberg: Berlin, Heidelberg, 2004; pp 169-273.
4. Bhushan, B.; Caspers, M., An overview of additive manufacturing (3D printing) for microfabrication. *Microsystem Technologies* **2017,** *23* (4), 1117-1124.
5. Miri, A. K.; Mirzaee, I.; Hassan, S.; Mesbah Oskui, S.; Nieto, D.; Khademhosseini, A.; Zhang, Y. S., Effective bioprinting resolution in tissue model fabrication. *Lab on a Chip* **2019,** *19* (11), 2019-2037.
6. Zhu, W.; Ma, X.; Gou, M.; Mei, D.; Zhang, K.; Chen, S., 3D printing of functional biomaterials for tissue engineering. *Current Opinion in Biotechnology* **2016,** *40*, 103-112.
7. Bhusal, A.; Dogan, E.; Nguyen, H.-A.; Labutina, O.; Nieto, D.; Khademhosseini, A.; Miri, A. K., Multi-material digital light processing bioprinting of hydrogel-based microfluidic chips. *Biofabrication* **2022,** *14* (1), 014103.
8. Tumbleston, J. R.; Shirvanyants, D.; Ermoshkin, N.; Janusziewicz, R.; Johnson, A. R.; Kelly, D.; Chen, K.; Pinschmidt, R.; Rolland, J. P.; Ermoshkin, A.; Samulski, E. T.; DeSimone, J. M., Continuous liquid interface production of 3D objects. *Science* **2015,** *347* (6228), 1349-1352.
9. Baldacchini, T., *Three-dimensional microfabrication using two-photon polymerization: fundamentals, technology, and applications*. William Andrew: 2015.
10. Lemma, E. D.; Spagnolo, B.; De Vittorio, M.; Pisanello, F., Studying Cell Mechanobiology in 3D: The Two-Photon Lithography Approach. *Trends in Biotechnology* **2019,** *37* (4), 358-372.
11. Gittard, S. D.; Narayan, R. J., Laser direct writing of micro- and nano-scale medical devices. *Expert review of medical devices* **2010,** *7* (3), 343-56.
12. Christina, S.; Deepak, M. K., Stereolithography. In *3D Printing*, Dragan, C., Ed. IntechOpen: Rijeka, 2018; p Ch. 1.
13. Stichel, T.; Hecht, B.; Houbertz, R.; Sextl, G., Two-Photon Polymerization as Methode for the Fabrication of Large Scale Biomedical Scaffold Applications. *Journal of Laser Micro / Nanoengineering* **2010,** *5*, 209-212.
14. Weisgrab, G.; Guillaume, O.; Guo, Z.; Heimel, P.; Slezak, P.; Poot, A.; Grijpma, D.; Ovsianikov, A., 3D Printing of large-scale and highly porous biodegradable tissue engineering scaffolds from poly(trimethylene-carbonate) using two-photon-polymerization. *Biofabrication* **2020,** *12* (4), 045036.
15. Hsieh, T. M.; Benjamin Ng, C. W.; Narayanan, K.; Wan, A. C. A.; Ying, J. Y., Three-dimensional microstructured tissue scaffolds fabricated by two-photon laser scanning photolithography. *Biomaterials* **2010,** *31* (30), 7648-7652.
16. Bernal, P. N.; Delrot, P.; Loterie, D.; Li, Y.; Malda, J.; Moser, C.; Levato, R., Volumetric Bioprinting of Complex Living-Tissue Constructs within Seconds. *Advanced Materials* **2019,** *31* (42), 1904209.
17. Pimpin, A.; Srituravanich, W., Review on micro-and nanolithography techniques and their applications. *Engineering Journal* **2012,** *16* (1), 37-56.

18. Shaw, J. M.; Gelorme, J. D.; LaBianca, N. C.; Conley, W. E.; Holmes, S. J., Negative photoresists for optical lithography. *IBM Journal of Research and Development* **1997,** *41* (1.2), 81-94.
19. Hunt, M.; Taverne, M.; Askey, J.; May, A.; Van Den Berg, A.; Ho, Y. D.; Rarity, J.; Ladak, S., Harnessing Multi-Photon Absorption to Produce Three-Dimensional Magnetic Structures at the Nanoscale. *Materials (Basel, Switzerland)* **2020,** *13* (3).
20. Jing, X.; Fu, H.; Yu, B.; Sun, M.; Wang, L., Two-photon polymerization for 3D biomedical scaffolds: Overview and updates. *Frontiers in Bioengineering and Biotechnology* **2022,** *10*.
21. Fischer, J.; Wegener, M., Three-dimensional optical laser lithography beyond the diffraction limit. *Laser & Photonics Reviews* **2013,** *7* (1), 22-44.
22. Boyd, R., Nonlinear Optics. *Elsvier* **2008**.
23. Zipfel, W. R.; Williams, R. M.; Webb, W. W., Nonlinear magic: multiphoton microscopy in the biosciences. *Nature Biotechnology* **2003,** *21* (11), 1369-1377.
24. Göppert-Mayer, M., Über Elementarakte mit zwei Quantensprüngen. *Annalen der Physik* **1931,** *401* (3), 273-294.
25. Lee, K.-S.; Kim, R.; Yang, D. Y.; Park, S., Advances in 3D nano/microfabrication using two-photon initiated polymerization. *Progress in Polymer Science - PROG POLYM SCI* **2008,** *33*, 631-681.
26. Tétreault, N.; von Freymann, G.; Deubel, M.; Hermatschweiler, M.; Pérez-Willard, F.; John, S.; Wegener, M.; Ozin, G., New Route to Three-Dimensional Photonic Bandgap Materials: Silicon Double Inversion of Polymer Templates. *Advanced Materials* **2006,** *18*.
27. Nguyen, A. K.; Gittard, S. D.; Koroleva, A.; Schlie, S.; Gaidukeviciute, A.; Chichkov, B. N.; Narayan, R. J., Two-photon polymerization of polyethylene glycol diacrylate scaffolds with riboflavin and triethanolamine used as a water-soluble photoinitiator. *Regenerative medicine* **2013,** *8* (6), 725-38.
28. Serbin, J.; Egbert, A.; Ostendorf, A.; Chichkov, B.; Houbertz, R.; Domann, G.; Schulz, J.; Cronauer, C.; Fröhlich, L.; Popall, M., Femtosecond Laser-Induced Two-Photon Polymerization of Inorganic Organic Hybrid Materials for Applications in Photonics. *Optics letters* **2003,** *28*, 301-3.
29. Li, L.; Fourkas, J. T., Multiphoton polymerization. *Materials Today* **2007,** *10* (6), 30-37.
30. Bhawalkar, J. D.; Kumar, N. D.; Zhao, C. F.; Prasad, P. N., Two-photon photodynamic therapy. *Journal of clinical laser medicine & surgery* **1997,** *15* (5), 201-4.
31. Sugioka, K.; Cheng, Y., REVIEW Ultrafast lasers—reliable tools for advanced materials processing. *Light: Science & Applications* **2014,** *3*, e149.
32. Tomazio, N.; Otuka, A.; Almeida, G.; Roselló-Mechó, X.; Andres, M. V.; Mendonça, C., Femtosecond laser fabrication of high-Q whispering gallery mode microresonators via two-photon polymerization. *Journal of Polymer Science Part B: Polymer Physics* **2017,** *55*.
33. Wu, S.; Wu, D.; Xu, J.; Hanada, Y.; Suganuma, R.; Wang, H.; Makimura, T.; Sugioka, K.; Midorikawa, K., Characterization and mechanism of glass microwelding by double-pulse ultrafast laser irradiation. *Optics Express* **2012,** *20* (27), 28893-28905.
34. Fischer, J.; Wegener, M., Three-dimensional optical laser lithography beyond the diffraction limit. *Laser & Photonics Review* **2013,** *7*, 22-44.
35. Zhou, X.; Hou, Y.; Lin, J., A review on the processing accuracy of two-photon polymerization. *AIP Advances* **2015,** *5*, 030701.
36. Jakubiak, J.; Rabek, J., Three-dimensional (3D) photopolymerization in stereolithography - Part I. Fundamentals of 3D photopolymerization. *Polimery/Polymers* **2000,** *45*, 759-770.

37. Hohmann, J.; Renner, M.; Waller, E.; von Freymann, G., Three-Dimensional μ-Printing: An Enabling Technology. *Advanced Optical Materials* **2015,** *3*, n/a-n/a.
38. Doraiswamy, A.; Jin, C.; Narayan, R. J.; Mageswaran, P.; Mente, P.; Modi, R.; Auyeung, R.; Chrisey, D. B.; Ovsianikov, A.; Chichkov, B., Two photon induced polymerization of organic-inorganic hybrid biomaterials for microstructured medical devices. *Acta biomaterialia* **2006,** *2* (3), 267-75.
39. Doraiswamy, A.; Ovsianikov, A.; Gittard, S. D.; Monteiro-Riviere, N. A.; Crombez, R.; Montalvo, E.; Shen, W.; Chichkov, B. N.; Narayan, R. J., Fabrication of microneedles using two photon polymerization for transdermal delivery of nanomaterials. *Journal of nanoscience and nanotechnology* **2010,** *10* (10), 6305-12.
40. Kimura, Y.; Tsuji, W.; Yamashiro, H.; Toi, M.; Inamoto, T.; Tabata, Y., In situ adipogenesis in fat tissue augmented by collagen scaffold with gelatin microspheres containing basic fibroblast growth factor. *Journal of tissue engineering and regenerative medicine* **2010,** *4* (1), 55-61.
41. Weiß, T.; Schade, R.; Laube, T.; Berg, A.; Hildebrand, G.; Wyrwa, R.; Schnabelrauch, M.; Liefeith, K., Two-Photon Polymerization of Biocompatible Photopolymers for Microstructured 3D Biointerfaces. *Advanced Engineering Materials* **2011,** *13* (9), B264-B273.
42. Koroleva, A.; Gill, A. A.; Ortega, I.; Haycock, J. W.; Schlie, S.; Gittard, S. D.; Chichkov, B. N.; Claeyssens, F., Two-photon polymerization-generated and micromolding-replicated 3D scaffolds for peripheral neural tissue engineering applications. *Biofabrication* **2012,** *4* (2), 025005.
43. Koroleva, A.; Gittard, S.; Schlie, S.; Deiwick, A.; Jockenhoevel, S.; Chichkov, B., Fabrication of fibrin scaffolds with controlled microscale architecture by a two-photon polymerization-micromolding technique. *Biofabrication* **2012,** *4* (1), 015001.
44. Ovsianikov, A.; Gruene, M.; Pflaum, M.; Koch, L.; Maiorana, F.; Wilhelmi, M.; Haverich, A.; Chichkov, B., Laser printing of cells into 3D scaffolds. *Biofabrication* **2010,** *2* (1), 014104.
45. Kufelt, O.; El-Tamer, A.; Sehring, C.; Schlie-Wolter, S.; Chichkov, B. N., Hyaluronic acid based materials for scaffolding via two-photon polymerization. *Biomacromolecules* **2014,** *15* (2), 650-9.
46. Timashev, P.; Bardakova, K.; Minaev, N.; Demina, T.; Sakharnova, T.; Mitroshina, E.; Akovantseva, A.; Koroleva, A.; Asyutin, D.; Pimenova, L.; Konovalov, N.; Akopova, T.; Solovieva, A.; Mukhina, I.; Vedunova, M.; Chichkov, B.; Bagratashvili, V., Compatibility of cells of the nervous system with structured biodegradable chitosan-based hydrogel matrices. *Applied Biochemistry and Microbiology* **2016,** *52*, 508-514.
47. Engelhardt, S.; Hoch, E.; Borchers, K.; Meyer, W.; Krüger, H.; Tovar, G. E. M.; Gillner, A., Fabrication of 2D protein microstructures and 3D polymer–protein hybrid microstructures by two-photon polymerization. *Biofabrication* **2011,** *3* (2), 025003.
48. Pitts, J.; Campagnola, P.; Epling, G.; Goodman, S., Submicron Multiphoton Free-Form Fabrication of Proteins and Polymers: Studies of Reaction Efficiencies and Applications in Sustained Release. *Macromolecules* **2000,** *33*.
49. Pitts, J.; Howell, A.; Taboada, R.; Banerjee, I.; Wang, J.; Goodman, S.; Campagnola, P., New Photoactivators for Multiphoton Excited Three-dimensional Submicron Cross-linking of Proteins: Bovine Serum Albumin and Type 1 Collagen¶†. *Photochemistry and photobiology* **2002,** *76*, 135-44.
50. Basu, S.; Rodionov, V.; Terasaki, M.; Campagnola, P., Multiphoton-excited microfabrication in live cells via Rose Bengal cross-linking of cytoplasmic proteins. *Optics letters* **2005,** *30*, 159-61.

51. Cunningham, L.; Veilleux, M.; Campagnola, P., Freeform multiphoton excited microfabrication for biological applications using a rapid prototyping CAD-based approach. *Optics express* **2006,** *14*, 8613-21.
52. Claeyssens, F.; Hasan, E.; Gaidukeviciute, A.; Achilleos, D.; Ranella, A.; Reinhardt, C.; Ovsianikov, A.; Shizhou, X.; Fotakis, C.; Vamvakaki, M.; Chichkov, B.; Farsari, M., Three-Dimensional Biodegradable Structures Fabricated by Two-Photon Polymerization. *Langmuir* **2009,** *25*, 3219-3223.
53. Gomez, N.; Schmidt, C., Nerve growth factor-immobilized polypyrrole: Bioactive electrically conducting polymer for enhanced neurite extension. *Journal of biomedical materials research. Part A* **2007,** *81*, 135-49.
54. Koroleva, A.; Deiwick, A.; Nguyen, A.; Schlie-Wolter, S.; Narayan, J.; Timashev, P.; Popov, V.; Bagratashvili, V.; Chichkov, B., Osteogenic Differentiation of Human Mesenchymal Stem Cells in 3-D Zr-Si Organic-Inorganic Scaffolds Produced by Two-Photon Polymerization Technique. *PloS one* **2015,** *10*, e0118164.
55. Skoog, S.; Nguyen, A.; Kumar, G.; Zheng, J.; Goering, P.; Koroleva, A.; Chichkov, B.; Narayan, J., Two-photon polymerization of 3-D zirconium oxide hybrid scaffolds for long-term stem cell growth. *Biointerphases* **2014,** *9*, 029014.
56. Vedunova, M. V.; Timashev, P. S.; Mishchenko, T. A.; Mitroshina, E. V.; Koroleva, A. V.; Chichkov, B. N.; Panchenko, V. Y.; Bagratashvili, V. N.; Mukhina, I. V., Formation of Neural Networks in 3D Scaffolds Fabricated by Means of Laser Microstereolithography. *Bulletin of Experimental Biology and Medicine* **2016,** *161* (4), 616-621.
57. Kaehr, B.; Allen, R.; Javier, D. J.; Currie, J.; Shear, J. B., Guiding neuronal development with in situ microfabrication. *Proceedings of the National Academy of Sciences* **2004,** *101* (46), 16104-16108.
58. Seidlits, S.; Schmidt, C.; Shear, J., High-Resolution Patterning of Hydrogels in Three Dimensions using Direct-Write Photofabrication for Cell Guidance. *Advanced Functional Materials* **2009,** *19*, 3543-3551.
59. Spivey, E. C.; Ritschdorff, E. T.; Connell, J. L.; McLennon, C. A.; Schmidt, C. E.; Shear, J. B., Multiphoton Lithography of Unconstrained Three-Dimensional Protein Microstructures. *Advanced Functional Materials* **2013,** *23* (3), 333-339.
60. Yuan, Y.; Chen, L.; Shi, Z.; Chen, J., Micro/Nanoarchitectonics of 3D Printed Scaffolds with Excellent Biocompatibility Prepared Using Femtosecond Laser Two-Photon Polymerization for Tissue Engineering Applications. *Nanomaterials* **2022,** *12*, 391.
61. Danilevicius, P.; Rekštyte, S.; Gadonas, R.; Malinauskas, M.; Balciunas, E.; Jarasiene, R.; Baltriukiene, D.; Bukelskiene, V.; Kraniauskas, A.; Sirmenis, R., Micro-structured polymer scaffolds fabricated by direct laser writing for tissue engineering. *BIOMEDO* **2012,** *17* (8), 081405.
62. Ovsianikov, A.; Deiwick, A.; Van Vlierberghe, S.; Dubruel, P.; Möller, L.; Dräger, G.; Chichkov, B., Laser Fabrication of Three-Dimensional CAD Scaffolds from Photosensitive Gelatin for Applications in Tissue Engineering. *Biomacromolecules* **2011,** *12*, 851-8.
63. Tomal, W.; Ortyl, J. Water-Soluble Photoinitiators in Biomedical Applications *Polymers* [Online], 2020.
64. Butkus, A.; Skliutas, E.; Gailevičius, D.; Malinauskas, M., Femtosecond-laser direct writing 3D micro/nano-lithography using VIS-light oscillator. *Journal of Central South University* **2022,** *29* (10), 3270-3276.
65. Albota, M.; Beljonne, D.; Brédas, J.-L.; Ehrlich, J. E.; Fu, J.-Y.; Heikal, A. A.; Hess, S. E.; Kogej, T.; Levin, M. D.; Marder, S. R.; McCord-Maughon, D.; Perry, J. W.; Röckel, H.; Rumi, M.; Subramaniam, G.; Webb, W. W.; Wu, X.-L.; Xu, C., Design of Organic Molecules with Large Two-Photon Absorption Cross Sections. *Science* **1998,** *281* (5383), 1653-1656.

66. Cumpston, B. H.; Ananthavel, S. P.; Barlow, S.; Dyer, D. L.; Ehrlich, J. E.; Erskine, L. L.; Heikal, A. A.; Kuebler, S. M.; Lee, I. Y. S.; McCord-Maughon, D.; Qin, J.; Röckel, H.; Rumi, M.; Wu, X.-L.; Marder, S. R.; Perry, J. W., Two-photon polymerization initiators for three-dimensional optical data storage and microfabrication. *Nature* **1999,** *398* (6722), 51-54.
67. He, G. S.; Tan, L.-S.; Zheng, Q.; Prasad, P. N., Multiphoton Absorbing Materials: Molecular Designs, Characterizations, and Applications. *Chemical Reviews* **2008,** *108* (4), 1245-1330.
68. Nguyen, A.; Narayan, R., Two-photon polymerization for biological applications. *Materials Today* **2017,** *20*.
69. Nazir, R.; Danilevicius, P.; Ciuciu, A. I.; Chatzinikolaidou, M.; Gray, D.; Flamigni, L.; Farsari, M.; Gryko, D. T., π-Expanded Ketocoumarins as Efficient, Biocompatible Initiators for Two-Photon-Induced Polymerization. *Chemistry of Materials* **2014,** *26* (10), 3175-3184.
70. Xing, H.; Wang, X.; Zhao, Y., Study on a series of water-soluble photoinitiators for fabrication of 3D hydrogels by two-photon polymerization. *Dyes and Pigments* **2017,** *141*.
71. Ovsianikov, A.; Mühleder, S.; Torgersen, J.; Li, Z.; Qin, X.-H.; Van Vlierberghe, S.; Dubruel, P.; Holnthoner, W.; Redl, H.; Liska, R.; Stampfl, J., Laser Photofabrication of Cell-Containing Hydrogel Constructs. *Langmuir* **2014,** *30* (13), 3787-3794.
72. Zhang, S.; Vijayavenkataraman, S.; Lu, W. F.; Fuh, J. Y. H., A review on the use of computational methods to characterize, design, and optimize tissue engineering scaffolds, with a potential in 3D printing fabrication. *Journal of Biomedical Materials Research Part B: Applied Biomaterials* **2019,** *107* (5), 1329-1351.
73. Baldacchini, T.; LaFratta, C. N.; Farrer, R. A.; Teich, M. C.; Saleh, B. E. A.; Naughton, M. J.; Fourkas, J. T., Acrylic-based resin with favorable properties for three-dimensional two-photon polymerization. *Journal of Applied Physics* **2004,** *95* (11), 6072-6076.
74. Kawata, S.; Sun, H.-B.; Tanaka, T.; Takada, K., Finer Features for Functional Microdevices. *Nature* **2001,** *412*, 697-8.
75. Brigo, L.; Urciuolo, A.; Giulitti, S.; Della Giustina, G.; Tromayer, M.; Liska, R.; Elvassore, N.; Brusatin, G., 3D high-resolution two-photon crosslinked hydrogel structures for biological studies. *Acta biomaterialia* **2017,** *55*, 373.
76. Ovsianikov, A.; Viertl, J.; Chichkov, B.; Oubaha, M.; MacCraith, B.; Sakellari, I.; Giakoumaki, A.; Gray, D.; Vamvakaki, M.; Farsari, M.; Fotakis, C., Ultra-Low Shrinkage Hybrid Photosensitive Material for Two-Photon Polymerization Microfabrication. *ACS Nano* **2008,** *2* (11), 2257-2262.
77. Jiaxi, S.; Michas, C.; Chen, C.; White, A.; Grinstaff, M., From Simple to Architecturally Complex Hydrogel Scaffolds for Cell and Tissue Engineering Applications: Opportunities Presented by Two-Photon Polymerization. *Advanced Healthcare Materials* **2019,** *9*.
78. Sanjuan-Alberte, P.; Vaithilingam, J.; Moore, J. C.; Wildman, R. D.; Tuck, C. J.; Alexander, M. R.; Hague, R. J. M.; Rawson, F. J. Development of Conductive Gelatine-Methacrylate Inks for Two-Photon Polymerisation *Polymers* [Online], 2021.
79. Miri, A. K.; Goodarzi Hosseinabadi, H.; Cecen, B.; Hassan, S.; Zhang, Y. S., Permeability Mapping of Gelatin Methacryloyl Hydrogels. *Acta biomaterialia* **2018,** *77*.
80. Tabata, Y., Biomaterial technology for tissue engineering applications. *Journal of the Royal Society, Interface / the Royal Society* **2009,** *6 Suppl 3*, S311-24.
81. Gopinathan, J.; Noh, I., Recent trends in bioinks for 3D printing. *Biomaterials Research* **2018,** *22* (1), 11.

82. Accardo, A.; Blatche, M.-C.; Courson, R.; Loubinoux, I.; Vieu, C.; Malaquin, L., Two-photon lithography and microscopy of 3D hydrogel scaffolds for neuronal cell growth. *Biomedical Physics & Engineering Express* **2018,** *4*.
83. Zhiganshina, E. R.; Arsenyev, M. V.; Chubich, D. A.; Kolymagin, D. A.; Pisarenko, A. V.; Burkatovsky, D. S.; Baranov, E. V.; Vitukhnovsky, A. G.; Lobanov, A. N.; Matital, R. P.; Aleynik, D. Y.; Chesnokov, S. A., Tetramethacrylic benzylidene cyclopentanone dye for one- and two-photon photopolymerization. *European Polymer Journal* **2022,** *162*, 110917.
84. Valente, F.; Hepburn, M. S.; Chen, J.; Aldana, A. A.; Allardyce, B. J.; Shafei, S.; Doyle, B. J.; Kennedy, B. F.; Dilley, R. J., Bioprinting silk fibroin using two-photon lithography enables control over the physico-chemical material properties and cellular response. *Bioprinting* **2022,** *25*, e00183.
85. Malinauskas, M.; Danilevičius, P.; Baltriukienė, D.; Rutkauskas, M.; Žukauskas, A.; Kairytė, Ž.; Bičkauskaitė, G.; Purlys, V.; Paipulas, D.; Bukelskienė, V., 3D artificial polymeric scaffolds for stem cell growth fabricated by femtosecond laser. *Lithuanian Journal of Physics* **2010,** *50* (1).
86. Kufelt, O.; El-Tamer, A.; Sehring, C.; Meißner, M.; Schlie-Wolter, S.; Chichkov, B., Water-soluble Photopolymerizable Chitosan Hydrogels for Biofabrication via Two-Photon Polymerization. *Acta biomaterialia* **2015,** *18*.
87. Heitz, J.; Plamadeala, C.; Wiesbauer, M.; Freudenthaler, P.; Wollhofen, R.; Jacak, J.; Klar, T. A.; Magnus, B.; Köstner, D.; Weth, A.; Baumgartner, W.; Marksteiner, R., Bone-forming cells with pronounced spread into the third dimension in polymer scaffolds fabricated by two-photon polymerization. *Journal of Biomedical Materials Research Part A* **2017,** *105* (3), 891-899.
88. Alsharhan, A. T.; Acevedo, R.; Warren, R.; Sochol, R. D., 3D microfluidics via cyclic olefin polymer-based in situ direct laser writing. *Lab on a Chip* **2019,** *19* (17), 2799-2810.
89. Velden, G.; Fan, D.; Staufer, U., Fabrication of a microfluidic device by using two-photon lithography on a positive photoresist. *Micro and Nano Engineering* **2020,** *7*, 100054.
90. Marino, A.; Tricinci, O.; Battaglini, M.; Filippeschi, C.; Mattoli, V.; Sinibaldi, E.; Ciofani, G., A 3D Real-Scale, Biomimetic, and Biohybrid Model of the Blood-Brain Barrier Fabricated through Two-Photon Lithography. *Small* **2018,** *14* (6), 1702959.
91. Tricinci, O.; De Pasquale, D.; Marino, A.; Battaglini, M.; Pucci, C.; Ciofani, G., A 3D Biohybrid Real-Scale Model of the Brain Cancer Microenvironment for Advanced In Vitro Testing. *Advanced Materials Technologies* **2020,** *5* (10), 2000540.
92. Wu, C.-Y.; Stoecklein, D.; Kommajosula, A.; Lin, J.; Owsley, K.; Ganapathysubramanian, B.; Di Carlo, D., Shaped 3D microcarriers for adherent cell culture and analysis. *Microsystems & Nanoengineering* **2018,** *4* (1), 21.
93. Chizari, S.; Udani, S.; Farzaneh, A.; Stoecklein, D.; Carlo, D. D.; Hopkins, J. B., Scanning two-photon continuous flow lithography for the fabrication of multi-functional microparticles. *Optics Express* **2020,** *28* (26), 40088-40098.
94. Cordeiro, A. S.; Tekko, I. A.; Jomaa, M. H.; Vora, L.; McAlister, E.; Volpe-Zanutto, F.; Nethery, M.; Baine, P. T.; Mitchell, N.; McNeill, D. W.; Donnelly, R. F., Two-Photon Polymerisation 3D Printing of Microneedle Array Templates with Versatile Designs: Application in the Development of Polymeric Drug Delivery Systems. *Pharmaceutical Research* **2020,** *37* (9), 174.
95. Ovsianikov, A.; Chichkov, B.; Mente, P.; Monteiro-Riviere, N.; Doraiswamy, A.; Narayan, J., Two Photon Polymerization of Polymer–Ceramic Hybrid Materials for Transdermal Drug Delivery. *International Journal of Applied Ceramic Technology* **2007,** *4*, 22-29.
96. Muamer, K.; Bückmann, T.; Stenger, N.; Thiel, M.; Wegener, M., On the feasibility of pentamode mechanical metamaterials. *Applied Physics Letters* **2012,** *100*.

97. van Kesteren, S.; Shen, X.; Aldeghi, M.; Isa, L., Printing on Particles: Combining Two-Photon Nanolithography and Capillary Assembly to Fabricate Multimaterial Microstructures. *Advanced Materials* **2023,** *35* (11), 2207101.
98. Jin, D.; Chen, Q.; Huang, T.-Y.; Huang, J.; Zhang, L.; Duan, H., Four-dimensional direct laser writing of reconfigurable compound micromachines. *Materials Today* **2019,** *32*.
99. Lemma, E.; Sergio, S.; Spagnolo, B.; Pisanello, M.; Algieri, L.; Coluccia, A.; Maffia, M.; Vittorio, M.; Pisanello, F., Tunable mechanical properties of stent-like microscaffolds for studying cancer cell recognition of stiffness gradients. *Microelectronic Engineering* **2018,** *190*.
100. Faraji Rad, Z.; Prewett, P. D.; Davies, G. J., High-resolution two-photon polymerization: the most versatile technique for the fabrication of microneedle arrays. *Microsystems & Nanoengineering* **2021,** *7* (1), 71.
101. Aldawood, F.; Andar, A.; Desai, S., A Comprehensive Review of Microneedles: Types, Materials, Processes, Characterizations and Applications. *Polymers* **2021,** *13*, 2815.
102. Aldawood, F. K.; Andar, A.; Desai, S. A Comprehensive Review of Microneedles: Types, Materials, Processes, Characterizations and Applications *Polymers* [Online], 2021.
103. Gittard, S. D.; Miller, P. R.; Boehm, R. D.; Ovsianikov, A.; Chichkov, B. N.; Heiser, J.; Gordon, J.; Monteiro-Riviere, N. A.; Narayan, R. J., Multiphoton microscopy of transdermal quantum dot delivery using two photon polymerization-fabricated polymer microneedles. *Faraday Discussions* **2011,** *149* (0), 171-185.
104. Goodarzi Hosseinabadi, H.; Bagheri, R.; Altstädt, V., Shear band propagation in honeycombs: numerical and experimental. *Rapid Prototyping Journal* **2018,** *24*, 00-00.
105. Goodarzi Hosseinabadi, H.; Bagheri, R.; Avila Gray, L.; Altstädt, V.; Drechsler, K., Plasticity in polymeric honeycombs made by photo-polymerization and nozzle based 3D-printing. *Polymer Testing* **2017,** *63*.
106. Miri, A. K.; Nieto, D.; Iglesias, L.; Goodarzi Hosseinabadi, H.; Maharjan, S.; Ruiz-Esparza, G. U.; Khoshakhlagh, P.; Manbachi, A.; Dokmeci, M. R.; Chen, S.; Shin, S. R.; Zhang, Y. S.; Khademhosseini, A., Microfluidics-Enabled Multimaterial Maskless Stereolithographic Bioprinting. *Advanced Materials* **2018,** *30* (27), 1800242.
107. Goodarzi Hosseinabadi, H.; Dogan, E.; Miri, A. K.; Ionov, L., Digital Light Processing Bioprinting Advances for Microtissue Models. *ACS Biomaterials Science & Engineering* **2022,** *8* (4), 1381-1395.
108. Zandrini, T.; Shan, O.; Parodi, V.; Cerullo, G.; Raimondi, M.; Osellame, R., Multi-foci laser microfabrication of 3D polymeric scaffolds for stem cell expansion in regenerative medicine. *Scientific Reports* **2019,** *9*.
109. Trautmann, A.; Rüth, M.; Lemke, H.-D.; Walther, T.; Hellmann, R., Two-photon polymerization based large scaffolds for adhesion and proliferation studies of human primary fibroblasts. *Optics & Laser Technology* **2018,** *106*.
110. Gittard, S.; Nguyen, A.; Obata, K.; Koroleva, A.; Narayan, J.; Chichkov, B., Fabrication of microscale medical devices by two-photon polymerization with multiple foci via a spatial light modulator. *Biomedical optics express* **2011,** *2*, 3167-78.
111. Paun, i. a.; Popescu, R. C.; Mustaciosu, C.; Zamfirescu, M.; Calin, B.; Mihailescu, M.; Maria, D.; Popescu, A.; Diana, C.; Sopronyi, M.; Luculescu, C., Laser-direct writing by two-photon polymerization of 3D honeycomb-like structures for bone regeneration. *Biofabrication* **2018,** *10*.
112. Schade, R.; Weiß, T.; Berg, A.; Schnabelrauch, M.; Liefeith, K., Two-Photon Techniques in Tissue Engineering. *The International journal of artificial organs* **2010,** *33*, 219-27.
113. Danilevicius, P.; Georgiadi, L.; Pateman, C. J.; Claeyssens, F.; Chatzinikolaidou, M.; Farsari, M., The effect of porosity on cell ingrowth into accurately defined, laser-made, polylactide-based 3D scaffolds. *Applied Surface Science* **2015,** *336*, 2-10.

114. Weiß, T.; Hildebrand, G.; Schade, R.; Liefeith, K., Two-Photon polymerization for microfabrication of three-dimensional scaffolds for tissue engineering application. *Engineering in Life Sciences* **2009,** *9*, 384-390.